Investigation of collisional parameters for rough spheres in fluidized beds

Yang, Lei; Padding, Johan; Kuipers, J.A.M.

DOI
10.1016/j.powtec.2016.12.090

Publication date
2017

Document Version
Final published version

Published in
Powder Technology

Powder Technology 316 (2017) 256–264

Contents lists available at ScienceDirect

Powder Technology

journal homepage: www.elsevier.com/locate/powtec

Investigation of collisional parameters for rough spheres in fluidized beds

Lei Yang, J.T. (Johan) Padding *, J.A.M. (Hans) Kuipers

Department of Chemical Engineering and Chemistry, Eindhoven University of Technology, 5600, MB, Eindhoven, The Netherlands

ARTICLE INFO

Article history:
Received 17 May 2016
Received in revised form 19 December 2016
Accepted 29 December 2016
Available online 30 December 2016

Keywords:
Fluidization
Rough particles
Rotation
Two-fluid model
Discrete particle model

ABSTRACT

The effect of normal restitution coefficient and friction coefficient on the hydrodynamics of a dense bubbling solid-gas fluidized bed is investigated using a two fluid model (TFM) based on our kinetic theory of granular flow (KTGF) for rotating frictional particles. A comparison between TFM simulations using the present KTGF model, and a simpler KTGF model for rapid flows of slightly frictional, nearly elastic spheres derived by Jenkins and Zhang [1], is carried out. The simulation results reveal that both the coefficient of normal restitution and friction coefficient play an important role in the homogeneity of the bubbling bed. The particle friction has a strong effect on the solids flow patterns and distribution, while the normal restitution coefficient has a relatively small effect on both. The present model also predicts a larger amount of energy dissipation caused by the inclusion of particle friction. The present KTGF model leads to better agreement with detailed discrete particle model (DPM) simulation results for the axial particle velocity profiles and solids volume fraction distribution.

1. Introduction

Gas-solid fluidized beds find a widespread application in processes involving combustion, separation, classification, and catalytic cracking [2]. Understanding the dynamics of fluidized beds is a key issue in improving efficiency, reliability and scale-up. Owning to enormous increase in computer power and algorithm development, fundamental modelling of multiphase reactors has become an effective tool.

In this work, an Euler-Euler approach (Kuipers et al. [3], Gidaspow [4]) is used. In Eulerian two fluid models (TFM), both the gas phase and the solid phase are treated as fully interpenetrating continua and are described by separate governing balance equations of mass and momentum. The challenge of this model is to establish an accurate hydrodynamic description of the solid phase. State-of-the-art closures have been obtained from the kinetic theory of granular flow (KTGF), initiated by Jenkins and Savage [5], Jenkins and Richman [6], Lun [7], and Nieuwland [8].

The original KTGF models of Jenkins and Savage [5], Jenkins and Richman [6] and Gidaspow [4] were derived for nearly elastic particles with translational motion only. In reality, however, granular materials are frictional. The roughness of the granular materials has been shown to have a significant effect on stresses at least in the quasi-static regime [9]. During collisions of rough particles, the particles can rotate due to the surface friction. Consequently, translational and rotational kinetic energies may exchange. Attempts to quantify the friction effect have been somewhat limited. Based on Lun and Savage [10], Walton [11] introduced coefficients of restitution associated with both the normal and tangential components of the velocity at the contact point. These coefficients can be measured by performing experiments with real particles [12–14]. Jenkins and Zhang [1] developed a simple kinetic theory for collisional flows of identical, slightly frictional, nearly elastic spheres. An effective restitution coefficient was given in terms of the collision parameters, namely the normal coefficient of restitution e, friction coefficient μ, and tangential coefficient of restitution β. This model is widely used in the study of the gas-solid fluidization [15–17]. Goldschmidt et al. [18] found that the effects of particle friction could not be replaced by using this effective (smaller) restitution coefficient. More recently, there have appeared some other works regarding the effect of particle friction. Van Wachem et al. [19] derived a simplified algebraic granular temperature equation. They found that this simplification does not lead to obvious differences in the simulation results, but reduces the computational time by about 20%. However, their model cannot be used for semi-dilute and dilute systems. The frictional kinetic model from Schneiderbauer et al. [20] is based the KTGF model from Agrawal et al. [21], which was originally developed for systems with mesoscale structures such as risers with particle clusters. This model includes closures for the solids stress tensor, which considers collisional, kinetic and frictional stress. However, as pointed out by themselves, this model lacks an explicit dependence on material properties of the particles. Berzi and Vescovi [22] found that the yield stress ratio of granular material can be theoretically predicted by the extended theory from Jenkins and Berzi [23], which reveals that the extended kinetic theory can obtain excellent agreement with numerical simulations on simple shearing of inelastic, frictional and frictionless particles. However, they also

* Corresponding author at: Process & Energy Department, Delft University of Technology, The Netherlands.
E-mail address: J.T.Padding@tudelft.nl (J.T.(J.) Padding).

http://dx.doi.org/10.1016/j.powtec.2016.12.090

pointed out that the relation between the shear rigidity and the interparticle friction is still lacking.

Yang et al. [24] developed a KTGF for rough spheres including particle friction and rotation, where the rheological properties of the solid phase are explicitly described in terms of the friction coefficient. This new model has been incorporated into our in-house two-fluid model (TFM) code for the modelling of dense gas-solid fluidized beds. This model has been validated for a bubbling fluidized bed by Yang et al. [25].

In this work, we employ the new KTGF model (called model A) and compare it with the effective model by Jenkins and Zhang (model B) to investigate the influence of friction coefficient and normal restitution coefficient on the properties of a gas-solid fluidized bed. Similar to previous studies in the literature [18,26], we will compare our results with detailed DPM simulation results, where DPM is used as an "independent" modelling framework to further validate our KTGF in TFM.

2. Numerical models

The two fluid model treats both phases as fully interpenetrating continua. The continuity equations for the gas and solid phases are given respectively by Eqs. (1) and (2). The corresponding momentum equations are given by Eqs. (3) and (4).

$$\frac{\partial\left(\varepsilon_g\rho_g\right)}{\partial t}+\frac{\partial}{\partial \mathbf{r}}\cdot\left(\varepsilon_g\rho_g\mathbf{v}_g\right)=0 \tag{1}$$

$$\frac{\partial(\varepsilon_s\rho_s)}{\partial t}+\frac{\partial}{\partial \mathbf{r}}\cdot(\varepsilon_s\rho_s\mathbf{v}_s)=0 \tag{2}$$

$$\frac{\partial\left(\varepsilon_g\rho_g\mathbf{v}_g\right)}{\partial t}+\nabla\cdot\left(\varepsilon_g\rho_g\mathbf{v}_g\mathbf{v}_g\right)=-\varepsilon_g\nabla P_g-\nabla\cdot\varepsilon_g\boldsymbol{\tau}_g+\varepsilon_g\rho_g\mathbf{g}-\beta_A\left(\mathbf{v}_g-\mathbf{v}_s\right) \tag{3}$$

$$\frac{\partial(\varepsilon_s\rho_s\mathbf{v}_s)}{\partial t}+\nabla\cdot(\varepsilon_s\rho_s\mathbf{v}_s\mathbf{v}_s)=-\nabla\cdot(P_s\mathbf{I}+\varepsilon_s\boldsymbol{\tau}_s)+\varepsilon_s\rho_s\mathbf{g}+\beta_A\left(\mathbf{v}_g-\mathbf{v}_s\right)-\varepsilon_s\nabla P_g \tag{4}$$

The gas and solid phases are coupled through the interphase momentum transfer coefficient β_A. To describe the solid phase, KTGF with friction is used. In this work, particle surface friction and rotation are considered explicitly. In order to describe the solid phase rheology thoroughly, an extra energy balance equation for the fluctuating rotational kinetic energy of the solids was derived by Yang et al. [24].

$$\frac{3}{2}\left[\frac{\partial(\varepsilon_s\rho_s\Theta_t)}{\partial t}+\nabla\cdot(\varepsilon_s\rho_s\mathbf{v}_s\Theta_t)\right]=-\nabla\mathbf{v}_s:(P_s\mathbf{I}+\varepsilon_s\boldsymbol{\tau}_s)-\varepsilon_s\nabla\cdot(-\kappa_t\nabla\Theta_t)-\gamma_t-3\beta_A\Theta_t \tag{5}$$

$$\frac{3}{2}\left[\frac{\partial(\varepsilon_s\rho_s\Theta_r)}{\partial t}+\nabla\cdot(\varepsilon_s\rho_s\mathbf{v}_s\Theta_r)\right]=-\varepsilon_s\nabla\cdot(-\kappa_{r1}\nabla\Theta_r-\kappa_{r2}\nabla\Theta_t)-\gamma_r \tag{6}$$

Definitions of the translational granular temperature Θ_t and rotational granular temperature Θ_r are $\Theta_t\equiv\langle C^2\rangle/3$, $\Theta_r\equiv I\langle\Omega^2\rangle/3m$, where I is the particle's moment of inertia. The full expressions for the constitutive equations are summarized in Table 1.

3. Model validation

3.1. Simulation settings

Comparisons between DPM and TFM simulation results will be presented to validate the newly-built kinetic theory. In the simulations, a no-slip wall boundary condition for side walls (left, right, front and back side of the rectangular domain) is used for the gas phase. At the bottom inlet, a uniform gas velocity is specified, whereas at the top outlet, atmospheric pressure (101,325 Pa) is prescribed. For the solid phase, a partial slip boundary condition is used for the side walls. A relation for the solids velocity gradient and an expression for the pseudo Fourier fluctuation energy flux at the wall have been given by Sinclair and Jackson [27]. At high solids volume fraction, we employed the frictional stress model from Srivastava and Sundaresan [30] to account for dense packing. The simulation settings are specified as follows in Table 2.

Table 1
Closure equations of the new kinetic theory of granular flow with friction (model A).

Solid pressure tensor: $P_s=\varepsilon_s\rho_s\Theta_t[1+2(1+e)\varepsilon_s g_0]$

Bulk viscosity: $\lambda_s=\frac{4}{3}\varepsilon_s\rho_s\sigma g_0(1+e)\sqrt{\frac{\Theta_t}{\pi}}$

Solid stress tensor: $\boldsymbol{\tau}_s=-\{(\lambda_s-\frac{2}{3}\mu_{t_s})(\nabla\cdot\mathbf{v}_s)\mathbf{I}+\mu_{t_s}[\nabla\mathbf{v}_s+(\nabla\mathbf{v}_s)^T]+\mu_{r_s}[\nabla\mathbf{v}_s-(\nabla\mathbf{v}_s)^T]\}$

Translational energy dissipation: $\gamma_t=\Theta_t g_0\rho_s\varepsilon_s^2\left\{\begin{array}{l}-\frac{192}{\sigma}\sqrt{\frac{\Theta_t}{\pi}}[\eta_1(1+\eta_1)-(2\lambda+1)\mathrm{A}_1\\+(\lambda+1)\mathrm{A}_2]+12\nabla\cdot\mathbf{v}_s[\eta_1(1+\eta_1)\\+5[(\lambda+1)\mathrm{A}_4-(2\lambda+1)\mathrm{A}_3]\end{array}\right\}$ (T1)

Rotational energy dissipation rate: $\gamma_r=\Theta_t g_0\rho_s\varepsilon_s^2\{-\frac{96}{\sigma}\sqrt{\frac{\Theta_t}{\pi}}(2.5\mathrm{A}_2-\lambda\mathrm{A}_1)+120\nabla\cdot\mathbf{v}_s(2.5\mathrm{A}_4-\lambda\mathrm{A}_3)\}$ (T2)

Translational shear viscosity: $\mu_{t_s}=\overline{\mu}(1+\mu_{t_{s,c}})+\frac{3}{5}\lambda_s,\mu_{t_{s,c}}=-\frac{4}{5}\varepsilon_s g_0[-6(2\lambda+1)\mathrm{A}_1+2\eta_1]$

Rotational shear viscosity: $\mu_{r_s}=-8(2\lambda+1)\sigma g_0\rho_s\varepsilon_s^2\mathrm{A}_1\sqrt{\frac{\Theta_t}{\pi}}$

Translational thermal conductivity: $\kappa_t=\overline{\kappa}_t(1+\kappa_{t_{s,c}})+\frac{3}{2}\lambda_s,\ \kappa_{t_{s,c}}=-\varepsilon_s g_0(2\eta_1-16(2\lambda+1)\mathrm{A}_1)$

Rotational thermal conductivity: $\kappa_{r1}=\overline{\kappa}_{r,1}=\rho\Theta_t(L_3/2L_1),\kappa_{r2}=\overline{\kappa}_{r,2}=\rho\Theta_t(L_2/2L_1)$,

$L_1=\frac{-32\varepsilon_s g_0}{25\sigma}\sqrt{\frac{\Theta_t}{\pi}}[50\mathrm{A}_2/\lambda-10\mathrm{A}_1-10\mathrm{A}_{11}/3-50(\lambda+1)(\lambda+2)\mathrm{A}_{12}/(3\lambda)+10(3\lambda+4)\mathrm{A}_9/3]$

$L_2=g_0\varepsilon_s\Theta_t[\frac{56\eta_1\lambda(\lambda+2)}{5(\lambda+1)}-60(1+4\eta_1)(2\mathrm{A}_3\lambda-5\mathrm{A}_4)]$

$L_3=(1+\frac{12}{5}g_0\varepsilon_s)\lambda\Theta_t[-\frac{8\eta_1(2+\lambda)}{3(1+\lambda)}+50(1+\eta_1)\mathrm{A}_3]$

Here, λ is the granular temperature ratio. The expressions for A_1, A_2, A_3, A_4, A_9, A_{11}, and A_{12} can be found in Appendix A. For spheres, $\lambda=2.5\Theta_r/\Theta_t,\eta_1=-(1+e)/2,\eta_2=-(1+\beta_0)/7$.

3.2. Results and discussion

3.2.1. Influence of normal restitution coefficient

Fig. 1 shows a comparison of time-averaged axial particle velocity and solids volume fraction using different normal restitution coefficients. In all cases a solids circulation pattern emerges, in which small bubbles increase rapidly in size due to coalescence. Consequently, a zone of increased bubble development, initially close to the wall, moves towards the center of bed with increasing height above the gas inlet. Zones with high solids volume fraction near the lateral walls and bottom of the bed are observed in both DPM and TFM model A, while no dense zone near the bed bottom is present in TFM model B. Particles appear to move upwards in regions of more intense bubble activity and downwards in regions of lesser bubble activity, which results in the formation of a pronounced global solids circulation pattern in all models. Both solids circulation pattern and distribution are not very sensitive with respect to the normal restitution coefficient. Comparing with

Table 2
Properties of particle and settings.

Parameters	DPM	TFM
Particle	Glass (ρ = 2526 kg/m^3), σ = 2 mm	Same
Initial bed height	0.15 m	Same
Domain size	0.15 × 0.012 × 0.48 m	Same
Initial bed voidage	0.403	Same
Grid number (x × y × z)	25 × 2 × 80	Same
Normal spring stiffness	k_n = 12.000 N/m	–
Particle-particle collision	e = 0.97, 0.9, β_0 = 0.33, μ = 0, 0.05, 0.15	Same
Particle-wall collision	e_w = 0.97, β_w = 0.33, μ_w = 0.1	–
Specularity coefficient	–	0.1
Simulation time	25 s	Same
Superficial gas velocity	2.27 m/s	Same
Drag relation	Ergun [28], and Wen & Yu [29]	Same
Frictional viscosity model	–	Srivastava and Sundaresan [30]
Flow solver time step	10^{-4} s	Same
Solid phase time step	10^{-5} s	10^{-4} s

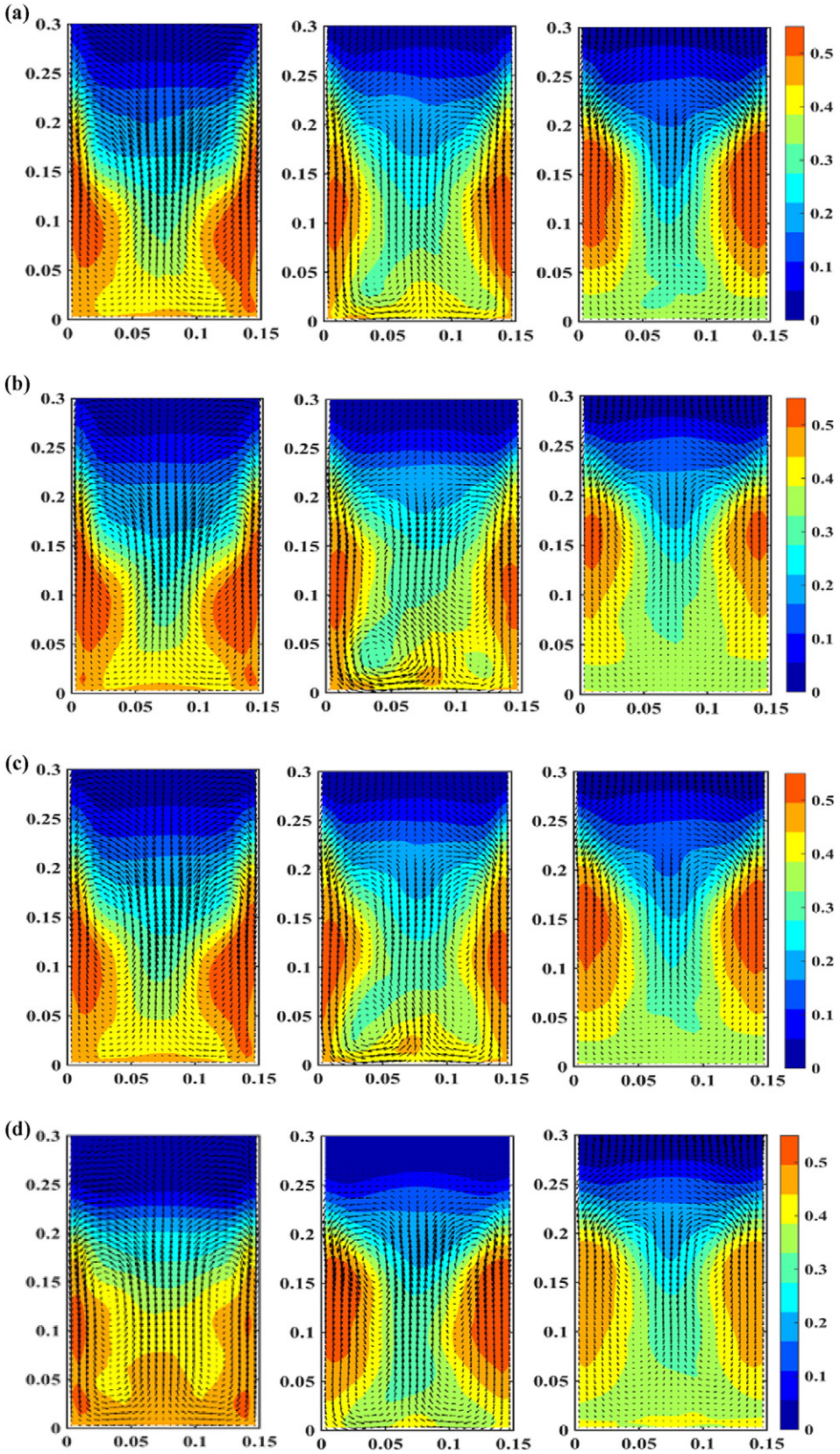

Fig. 1. Comparison of solid circulation pattern and solids volume fraction with a friction coefficient of 0.15 and 0.05. Left column: DPM model, Middle column: present TFM model A, Right column: TFM model B from Jenkins and Zhang. (a): $e = 0.80, \beta_0 = 0.33, \mu = 0.15$, (b): $e = 0.90, \beta_0 = 0.33, \mu = 0.15$, (c): $e = 0.97, \beta_0 = 0.33, \mu = 0.15$, (d): $e = 0.97, \beta_0 = 0.33, \mu = 0.05$.

DPM simulations, it is observed that both TFM models underpredict the axial particle velocity in the center, and TFM model A overpredicts it at the bottom. Comparing figures (c) and (d), decreasing the friction coefficient has significant influence on both the solids circulation pattern, i.e. velocity magnitude in the center and solids distribution, which indicates that friction coefficient plays important role in bubble

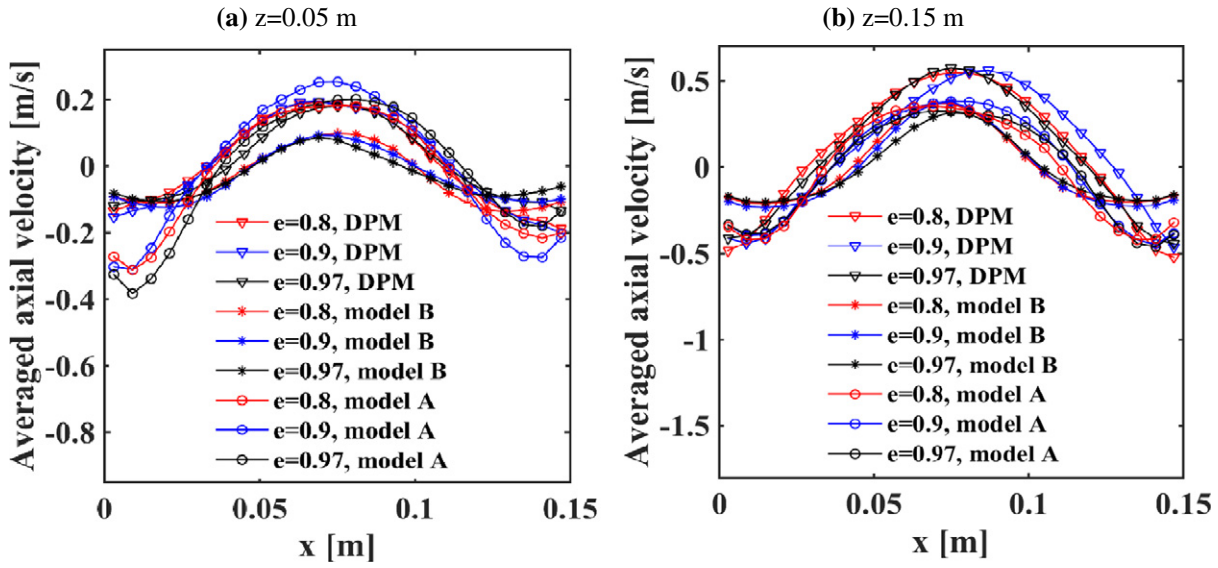

Fig. 2. Comparison of time-averaged axial particle velocity at heights 0.05 m (left) and 0.15 m (right) for $\beta_0 = 0.33, \mu = 0.15$ and various values of normal coefficient of restitution e (see legend).

motion. From Fig. 1(d), it seems that DPM simulation results are more sensitive to the frictional coefficient. Finally, it can be seen that in most cases TFM model A produces a somewhat better agreement with the DPM simulations than TFM model B.

Fig. 2 shows the time-averaged axial particle velocities using different normal restitution coefficients at two different heights. At a height of 0.05 m, TFM model A overpredicts the particle axial velocity near the wall but produces an excellent match with DPM simulation in the bulk. This is possibly due to different boundary conditions used in TFM versus DPM simulations. In our DPM model, we treat particle-wall collisions individually through a linear spring-dashpot model using three collisional parameters, which describes the result of particle-wall interactions quite accurately. However, in absence of TFM wall boundary conditions that include the rotational granular temperature, in the TFM simulations the popular boundary conditions from Sinclair and Jackson [27] are employed. Here a "specularity coefficient" is applied to characterize the amount of momentum and energy transfer due to collisions between particles and wall. However, these boundary conditions do not take into account the precise particle-wall frictional effects. On the contrary, the TFM model B underpredicts the particle axial velocity in the bulk and obtains good agreement with DPM simulation near the wall. At a height of 0.15 m, although both TFM models underestimate the particle axial velocity in the center, model A agrees well with DPM simulation near the wall. All these results correspond to the macroscopic solids circulation patterns shown in Fig. 1. It can be observed that increasing the normal restitution coefficient results only in slight changes in the particle axial velocity, i.e. a small decrease close to the wall.

Fig. 3 shows the energy dissipation rate of both TFM models for different normal restitution coefficients. Model A generally predicts a higher energy dissipation rate with increasing solids concentration. However, the calculated energy dissipation rate from model B first increases, reaches a maximum, then decreases, and finally keeps a plateau. With decreasing normal restitution coefficient, it can be seen that more energy is dissipated in particle-particle collisions for both models, especially in the region of solids concentration 0–0.3. In region of solids concentration 0.3–0.58, increasing the normal restitution coefficient leads to larger changes in model B than in model A. This is due to the different expressions for the energy dissipation rate γ. In model B, γ is proportional to $(1\text{-}e^2)$, which is not true in model A, as can be seen from Eq. (T1). However, both expressions have two terms. The first term relates to the collisional rate of kinetic energy interchange. It incorporates the energy dissipation from inelasticity and particle surface friction. The second term includes the particle velocity divergence. The resulting energy dissipation is the competition of these two terms. Furthermore, a small amount of energy is dissipated by particle rotation in model A. For rough particles ($\mu = 0.15$), the kinetic energy is transformed into rotation and subsequently less energy is dissipated in collisions. Nevertheless, model A predicts a larger amount of energy dissipation than model B in dense regions.

3.2.2. Influence of friction coefficient

Fig. 4 shows some instantaneous snapshots of bubble patterns obtained by the different models. Small bubbles are generated at the bottom and the wall, then grow in size due to coalescence, move towards

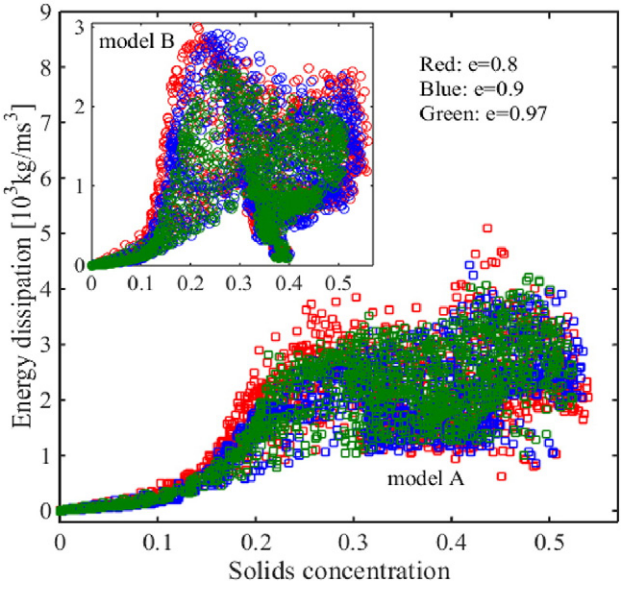

Fig. 3. Time-averaged (5–25 s) energy dissipation rate versus local solids concentration for different normal restitution coefficients predicted by model A (main plot) and model B (subplot) ($\beta_0 = 0.33, \mu = 0.15$).

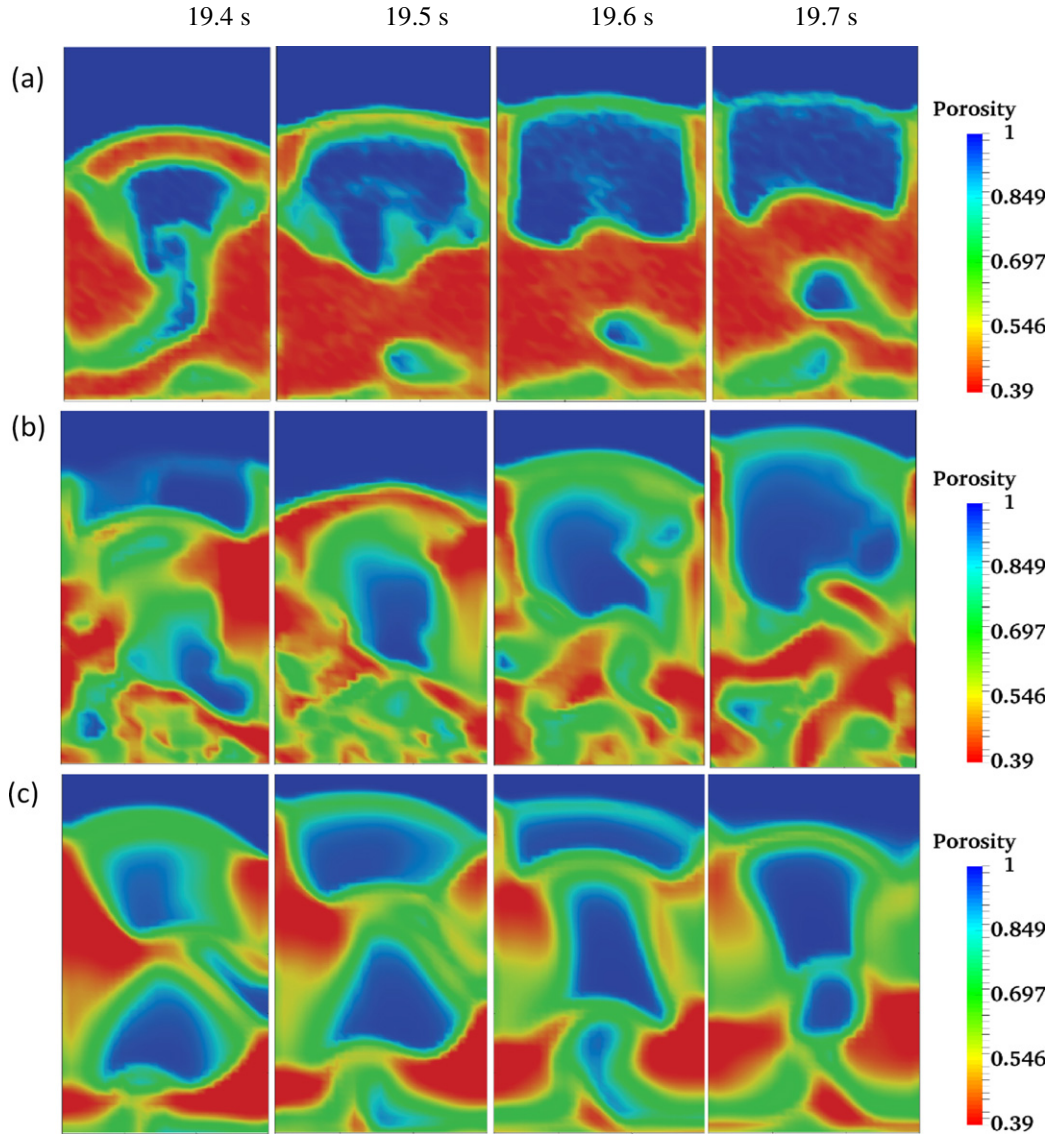

Fig. 4. Instantaneous snapshots of porosity from different simulations. Top row: DPM simulation, Middle row: TFM model A, Bottom row: TFM model B. For all cases $e = 0.9, \beta_0 = 0.33, \mu = 0.15$.

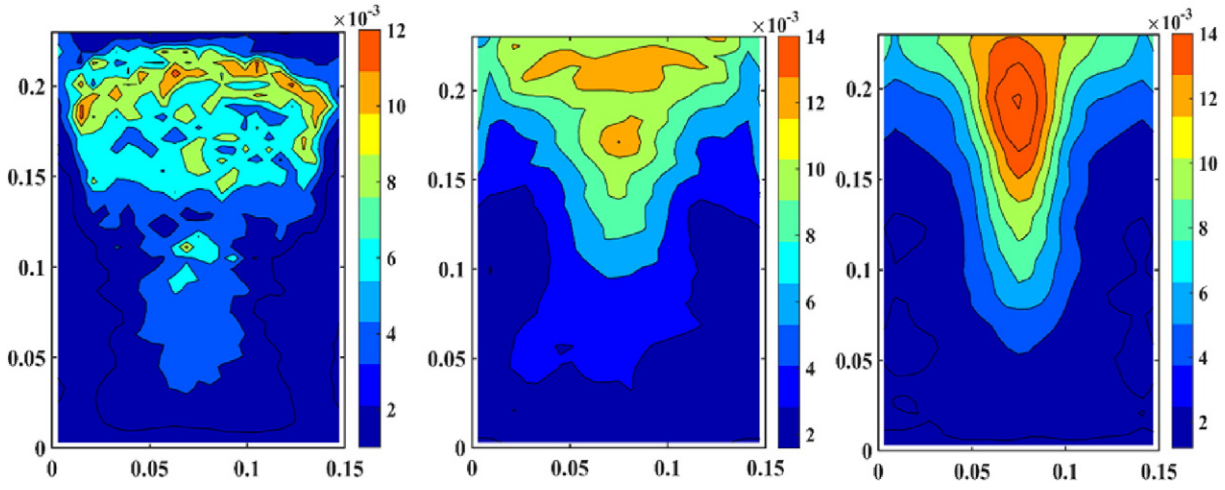

Fig. 5. Comparison of time averaged (5–25 s) translational granular temperature ($e = 0.97, \beta_0 = 0.33, \mu = 0$). Left: DPM simulation, Middle: TFM model A, Right: TFM model B.

the center [31], and finally burst through the bed surface. Because of the inclusion of particle surface friction and rotation, our present model A predicts a slightly more heterogeneous flow field than TFM model B. We note that in the TFM models (both A and B) larger bubbles and larger densely packed regions are formed than in the DPM model. However, the snapshots also show that the high density structures in TFM model A are more likely to span the entire width of the system than in TFM model B. This tendency towards slugging fluidization of TFM model A agrees better with the DPM simulations than TFM model B.

Fig. 5 shows a comparison of the distribution of translational granular temperature predicted by three models. In each computational cell of the DPM simulation, we first determine the averaged translational and rotational particle velocities of all particles located in that cell. Then, the translational and rotational granular temperatures in that cell are calculated based on the fluctuating velocities of each particle located in the same cell. From the figure, it can be seen that both TFM models predict a high granular temperatures above the bed surface (height above 0.22 m), while the DPM simulation predicts a very low granular temperature. This is an artefact caused by the fact that too few particles are present per computational cell and therefore often (in case of a single particle in a cell) a zero fluctuating velocity is determined in DPM in the region above 0.22 m. On the contrary, TFM is working with continuous fields, and a granular temperature is simulated even in these very dilute regions. Neglecting this region, the zones with high translational granular temperature are situated mainly at the top of the bed, away from the side walls in all simulations. TFM model A predicts a larger zone of translational granular temperature (0.008–0.001 m^2/s^2) than model B, which is influenced by the fact that particle rotation and friction are not yet included in the boundary conditions for rough side walls in Model A, therefore energy dissipation during particle-wall collisions is underestimated. However, model B predicts higher granular temperature in the up center of the bed than model A. The translational granular temperature in all cases has a similar distribution (below 0.22 m) and the overall magnitude of translational granular temperature matches well.

Fig. 6 shows contour plots of the rotational granular temperatures of TFM model A and DPM. The rotational granular temperature in TFM model A shows an almost uniform distribution in the bed, but the overall magnitude agrees to a reasonable extent, except for the case without friction. In this case, the wall serves as a source for particle rotation. The rotational granular temperature increases with increasing friction coefficient in both models. TFM model A obtains better agreement with DPM for larger friction coefficient. The reason for the almost uniform distribution of the rotational granular temperature in model A can be due to two major assumptions made in the current version of KTGF. Firstly, the mean rotational velocity is assumed to be zero, which means that in the modelling of particle rotation only the rotational energy balance equation is solved. Secondly, the gradient of the rotational granular temperature at the wall is assumed to be zero (corresponding to adiabatic walls for rotational granular temperature). We are currently working on improved boundary conditions, relaxing the latter limitation.

Fig. 7 shows a comparison of the time-averaged axial particle flux for different friction coefficients. The axial flux is negative near the wall and positive in the center, which indicates that particles move upward in the center and move down near the wall. The simulated particle axial flux

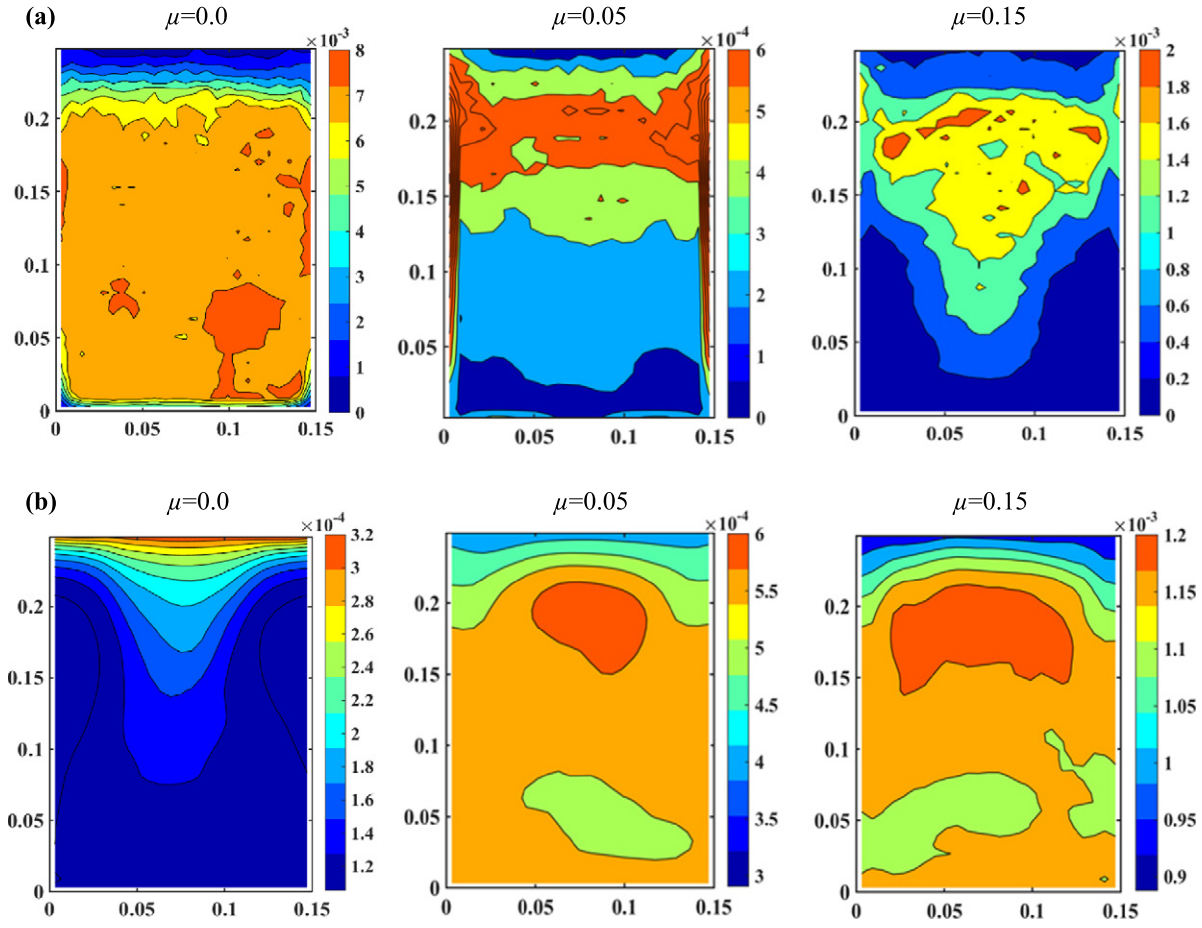

Fig. 6. Contour plots of time-averaged (5–25 s) and solids concentration weighted rotational granular temperature (m^2/s^2) for three friction coefficients (in all cases $e = 0.97, \beta_0 = 0.33$). (a, top row): DPM simulation, (b, bottom row): present TFM model A. No rotational temperature is present in TFM model B.

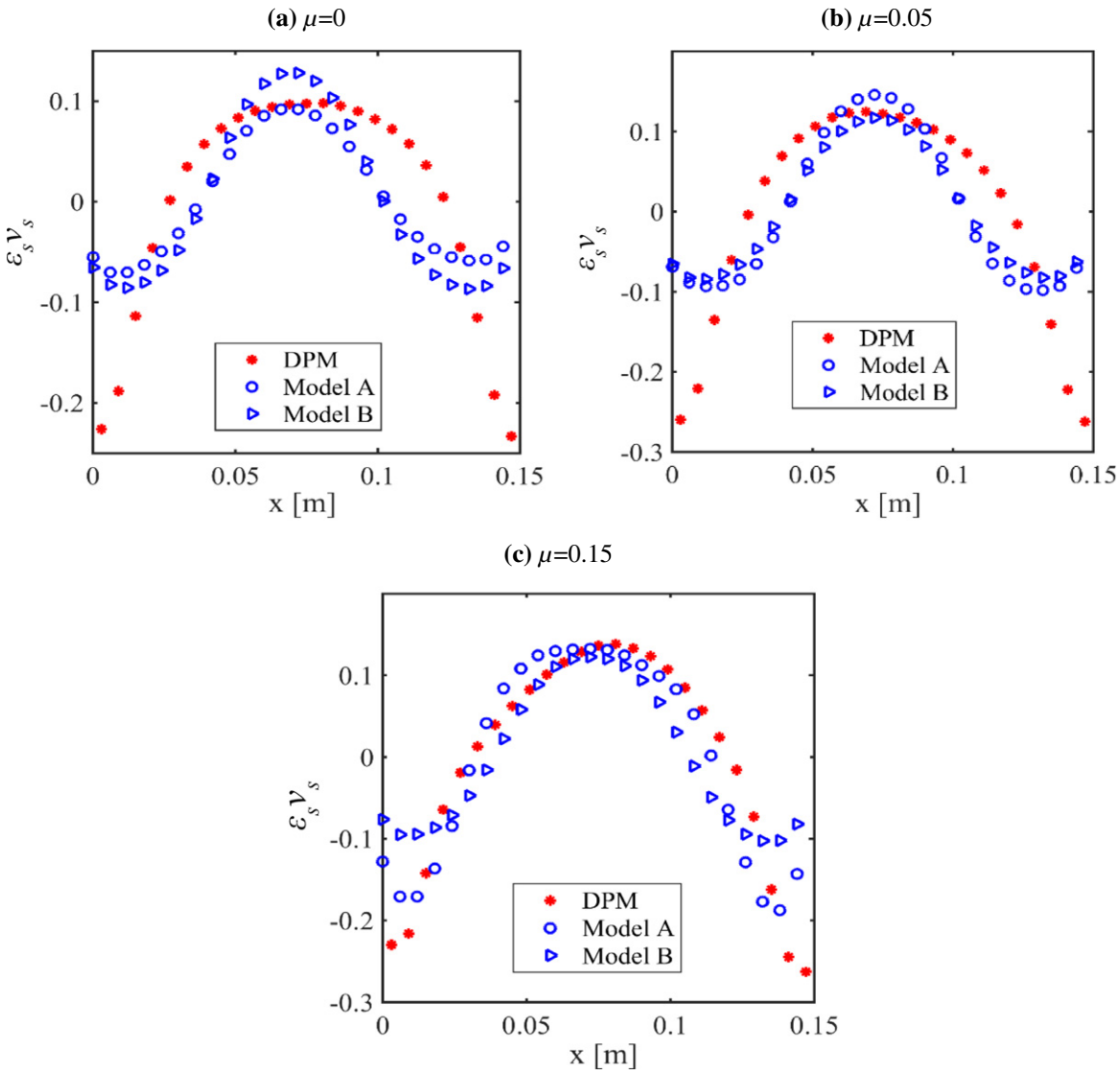

Fig. 7. Comparison of time-averaged (5–25 s) axial particle flux ($\varepsilon_s v_s$) at z = 0.15 m for different friction coefficients. In all cases $e = 0.90, \beta_0 = 0.33$.

from both TFM models A and model B underpredict the downward velocity near the wall. TFM model A obtains an excellent agreement with DPM at a friction coefficient of 0.15, except for small deviations for the flux near the wall. This is due to the fact that slug fluidization happens in model A, and more particles are pushed to the wall, leading to a strong slip velocity. The maximum down-flow flux is close to the wall in TFM models while it is at the wall in DPM model. As mentioned before, the phenomena are due to fact that a heuristic boundary conditions for particle slip velocity is employed in TFM simulations. By contrast, particle-wall collisions are considered realistically in DPM simulations. Although the predictions for the velocity profiles are similar for models A and B, it can be seen that for large friction TFM model A has a better agreement with the DPM simulations than model B.

Fig. 8 shows the distribution of energy dissipation rate measured in TFM models A and B as a function of the solids concentration. The simulated energy dissipation rate from both models increases with increasing solids concentration from 0 to 0.3, decreases when the solids concentration is in the range of 0.3–0.4, and finally reaches a plateau. Without friction, both TFM models predict almost the same energy dissipation rate. The new model A predicts a larger amount of energy dissipation with increasing friction coefficient. As has been pointed out, energy dissipation is the combination of a term related to collisional rate and the term due to compression of the granular medium. Model A considers not only the particle surface friction but also particle rotation. As a result, model A predicts a larger amount of energy dissipation. Simply, comparing figures (a), (b) and (c) for model A, with increasing particle friction there are more collisions between particles and thus more energy is dissipated.

4. Conclusions

In this work, we investigated the effects of normal restitution coefficient and friction coefficient on the hydrodynamics of a dense solid-gas fluidized bed, using a two fluid model (TFM) based on our recent kinetic theory of granular flow (KTGF) for rotating rough particles. The simulation results reveal that the coefficient of normal restitution and friction coefficient play important roles in the homogeneity of a bubbling bed. Variation of the normal restitution coefficient can slightly influence the time-averaged solids distribution and the gas-solids flow field. More energy is dissipated for more inelastic particles. However, the friction coefficient has a stronger effect on the solids flow patterns and distribution. The new KTGF model predicts a larger amount of energy dissipation caused by explicit inclusion of particle friction. With increasing friction coefficient, not only a larger amount of energy dissipation is

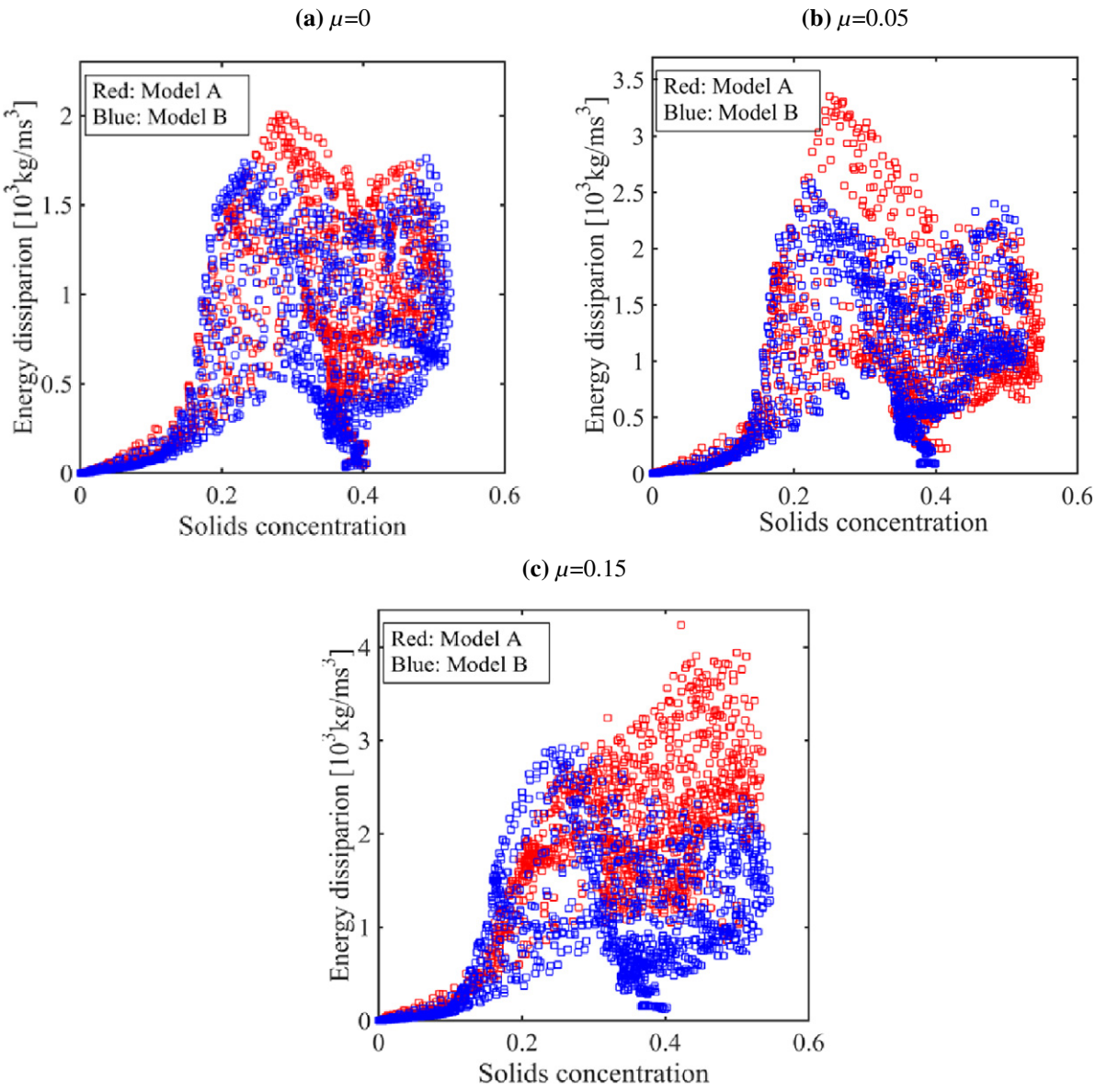

Fig. 8. Time-averaged (5–25 s) energy dissipation rate versus solids concentration for TFM models A and B and different friction coefficients. In all cases $e = 0.90$, $\beta_0 = 0.33$.

calculated but also the bed expands more rigorously as can be observed in animations of the simulations. Comparing with detailed DPM simulations, the present KTGF model leads to better agreement with DPM simulations for the axial particle velocity profiles and solids volume fraction distribution.

Nomenclature

I	moment of inertia, kg m^2
m	mass of the particle, kg
U_{mf}	minimum fluidization velocity, m/s
e	normal restitution coefficient

Greek letters

$\overline{\omega}$	magnitude of mean rotational velocity, rad/s
ρ	density, kg/m^3
Θ	granular temperature, m^2/s^2
β_0	tangential restitution coefficient
σ	particle diameter, m
γ	energy dissipation rate, J/(sm^3)
β_A	inter-phase momentum transfer coefficient, J/(sm^3)
$\boldsymbol{\tau}$	stress tensor, Pa
ε	volume fraction
κ	pseudo thermal conductivity, kg/(m·s)
μ_t	translational shear viscosity, kg/(m·s)

Subscript

s	solid phase
g	gas phase
r	rotational contribution
t	translational contribution

Acknowledgment

The authors thank the European Research Council for its financial support, under its Advanced Investigator Grant scheme, Contract no. 247298 (Multi-scale Flows).

Appendix A

All the basic integrals which could be solved analytically using Mathematica, are listed as follows,

$a_1 = (1+\lambda)\int_{\theta^*}^{\pi/2} \frac{\sin^2\theta_u \cos^2\theta_u}{(1+\lambda\cos^2\theta_u)^3} d\theta_u$

$a_2 = (1+\lambda)\int_{\theta 0}^{\theta^*} \frac{\sin^3\theta_u \cos\theta_u}{(1+\lambda\cos^2\theta_u)^3} d\theta_u$

$a_3 = (1+\lambda)\int_{\theta^*}^{\pi/2} \frac{\sin\theta_u \cos^3\theta_u}{(1+\lambda\cos^2\theta_u)^3} d\theta_u$

$a_4 = (1+\lambda)^{3/2}\int_{\theta^*}^{\pi/2} \frac{\sin^2\theta_u \cos^3\theta_u}{(1+\lambda\cos^2\theta_u)^{7/2}} d\theta_u$

$a_5 = (1+\lambda)^{3/2}\int_{0}^{\theta^*} \frac{\sin^3\theta_u \cos^2\theta_u}{(1+\lambda\cos^2\theta_u)^{7/2}} d\theta_u$

$a_6 = (1+\lambda)^{3/2}\int_{\theta^*}^{\pi/2} \frac{\cos^4\theta_u \sin\theta_u}{(\lambda\cos^2\theta_u+1)^{7/2}} d\theta_u$

$a_{10} = (1+\lambda)\int_{\theta^*}^{\pi/2} \frac{\sin^3\theta_u \cos^3\theta_u}{(1+\lambda\cos^2\theta_u)^4} d\theta_u$

$a_{14} = (1+\lambda)\int_{0}^{\theta^*} \frac{\sin^5\theta_u \cos\theta_u}{(1+\lambda\cos^2\theta_u)^4} d\theta_u$

$a_{17} = \int_{\theta^*}^{\pi/2} \frac{\sin^2\theta_u \cos^2\theta_u}{(1+\lambda\cos^2\theta_u)^4} d\theta_u$

$A_1 = -(\mu\eta_1 a_1 + \eta_2 a_2)$

$A_2 = (1+\lambda)[(\mu\eta_1)^2 a_3 + (\eta_2)^2 a_2]$

$A_3 = -(\mu\eta_1 a_4 + \eta_2 a_5)$

$A_4 = (1+\lambda)[(\mu\eta_1)^2 a_6 + (\eta_2)^2 a_5]$

$A_9 = -(\mu\eta_1 a_{17} + \eta_2 a_{16})$

$A_{11} = (\mu\eta_1)^2 a_{10} + (\eta_2)^2 a_{14}$

$A_{12} = (\mu\eta_1)^2 a_{15} + (\eta_2)^2 a_{16}$

References

[1] J.T. Jenkins, C. Zhang, Kinetic theory for identical, frictional, nearly elastic spheres, Phys. Fluids 14 (2002) 1228–1235.
[2] J.F. Davidson, R. Cliff, D. Harrison, Fluidization, second ed. Academic Press, London, UK, 1985.
[3] J.A.M. Kuipers, K.J. van Duin, F.P.H. van Beckum, W.P.M. van Swaaij, A numerical model of gas-fluidized beds, Chem. Eng. Sci. 47 (1992) 1913–1924.
[4] D. Gidaspow, Multiphase Flow and Fluidization: Continuum and Kinetic Theory Descriptions, Academic Press Inc., Boston, 1994.
[5] J.T. Jenkins, S.B. Savage, A theory for the rapid flow of identical, smooth, nearly elastic, spherical particles, J. Fluid Mech. 30 (1983) 187–202.
[6] J.T. Jenkins, M.W. Richman, Grad's 13-moment system for a dense gas of inelastic spheres, Arch. Rotational Mech. Anal. 87 (1985) 355–377.
[7] C.K.K. Lun, Kinetic theory for granular flow of dense, slightly inelastic, slightly rough spheres, J. Appl. Mech. 233 (1991) 539–559.
[8] J.J. Nieuwland, Hydrodynamic Modelling of Gas-Solid Two-phase Flows(Ph.D. thesis) Twente University, Enschede, the Netherlands, 1995.
[9] J. Sun, S. Sundaresan, A constitutive model with microstructure evolution for flow of rate-independent granular materials, J. Fluid Mech. 682 (2011) 590–616.
[10] C.K.K. Lun, S.B. Savage, A simple kinetic theory for granular flow of rough, inelastic, spherical particles, J. Appl. Mech. 54 (1987) 47–53.
[11] O.R. Walton, Numerical simulation of inelastic, frictional particle-particle interactions, Particulate Two-phase Flow 1993, p. 25.
[12] S.F. Foerster, M.Y. Louge, H. Chang, K. Allia, Measurements of the collision properties of small spheres, Phys. Fluids 6 (1994) 1108.
[13] A. Lorenz, C. Tuozzolo, M. Louge, Measurements of impact properties of small, nearly spherical particles, Exp. Mech. 37 (1997) 292–298.
[14] A. Kharaz, D. Gorham, A. Salman, An experimental study of the elastic rebound of spheres, Powder Technol. 120 (2001) 281–291.
[15] M.J.V. Goldschmidt, R. Beetstra, J.A.M. Kuipers, Hydrodynamic modelling of dense gas-fluidized beds: comparison and validation of 3D discrete particle and continuum models, Powder Technol. 142 (2004) 23–47.
[16] J. Sun, F. Battaglia, Hydrodynamic modeling of particle rotation for segregation in bubbling gas-fluidized beds, Chem. Eng. Sci. 61 (2006) 1470–1479.
[17] V. Verma, N.G. Deen, J.T. Padding, J.A.M. Kuipers, Two-fluid modeling of three-dimensional cylindrical gas-solid fluidized beds using the kinetic theory of granular flow, Chem. Eng. Sci. 102 (2013) 227–245.
[18] M.J.V. Goldschmidt, J.A.M. Kuipers, W.P.M. van Swaaij, Hydrodynamic modeling of dense gas-fluidised beds using the kinetic theory of granular flow: effect of coefficient of restitution on bed dynamics, Chem. Eng. Sci. 56 (2001) 571–578.
[19] B.G.M. Van Wachem, J.C. Schouten, C.M. Van den Bleek, R. Krishna, J.L. Sinclair, Comparative analysis of CFD models of dense gas-solid systems, AIChE J. 47 (2001) 1035–1051.
[20] S. Schneiderbauer, A. Aigner, S. Pirker, A comprehensive frictional-kinetic model for gas-particle flows: analysis of fluidized and moving bed regimes, Chem. Eng. Sci. 80 (2012) 279–292.
[21] K. Agrawal, P.N. Loezos, M. Syamlal, S. Sundaresan, The role of meso-scale structures in rapid gas-solid flows, J. Fluid Mech. 445 (2001) 151–185.
[22] D. Berzi, D. Vescovi, Different singularities in the functions of extended kinetic theory at the origin of the yield stress in granular flows, Phys. Fluids 27 (2015) 013302.
[23] J.T. Jenkins, D. Berzi, Dense inclined flows of inelastic spheres: tests of an extension of kinetic theory, Granul. Matter 12 (2010) 151–158.
[24] L. Yang, J.T. Padding, J.A.M. Kuipers, Modification of kinetic theory of granular flow for frictional spheres, part I: two-fluid model derivation and numerical implementation, Chem. Eng. Sci. 152 (2016) 767–782.
[25] L. Yang, J.T. Padding, J.A.M. Kuipers, Modification of kinetic theory of granular flow for frictional spheres, part II: model validation, Chem. Eng. Sci. 152 (2016) 783–794.
[26] G.A. Bokkers, M. van Sint Annaland, J.A.M. Kuipers, Comparison of Continuum Models Using the Kinetic Theory of Granular Flow With Discrete Particle Models and Experiments: Extent of Particle Mixing Induced by Bubbles, 2004 187–194.
[27] J. Sinclair, R. Jackson, Gas-particle flow in a vertical pipe with particle-particle interactions, AICHE J. 35 (1989) 1473.
[28] S. Ergun, Fluid flow through packed columns, Chem. Eng. Prog. 48 (1952) 89–94.
[29] C.Y. Wen, Y.H. Yu, A generalized method for predicting the minimum fluidization velocity, AICHE J. 12 (1966) 610–612.
[30] A. Srivastava, S. Sundaresan, Analysis of a frictional-kinetic model for gas-particle flow, Powder Technol. 129 (2003) 72–85.
[31] D. Kunii, O. Levenspiel, Fluidization Engineering, second ed. Butterworth-Heinemann, Boston, 1991.